Hindawi
Journal of Nanomaterials
Volume 2019, Article ID 2707909, 7 pages
https://doi.org/10.1155/2019/2707909

Research Article

Fabrication of Reduced Graphene Oxide-Ag Nanocomposites and Analysis on the Interaction with BSA

Huali Zhang,[1] Wen Liu,[2] Linqing Yang,[3] Jun Liu,[4] Yunfei Wang,[3] Xuyan Mao,[4] Jing Wang,[5] and Xiangyu Xu[4]

[1]*Collaborative Innovation Center for Birth Defect Research and Transformation of Shandong Province, Jining Medical University, Jining 272067, Shandong Province, China*
[2]*College of Basic Medical, Jining Medical University, Jining 272067, Shandong Province, China*
[3]*Program for Scientific Research Innovation Team in Precision Medicine of Gynecologic Oncology, Affiliated Hospital of Jining Medical University, Jining 272067, Shandong Province, China*
[4]*Laboratory of New Antitumor Drug Molecular Design & Synthesis, College of Basic Medical, Jining Medical University, Jining 272067, Shandong Province, China*
[5]*Department of Physics and Information Engineering, Jining University, Qufu 273155, Shandong Province, China*

Correspondence should be addressed to Jing Wang; wangjingouc@jnxy.edu.cn and Xiangyu Xu; xuxiangyu1212@163.com

Received 9 July 2019; Accepted 28 September 2019; Published 18 November 2019

Academic Editor: Zafar Iqbal

Graphene is an excellent platform to support and stabilize silver nanoparticles (AgNPs). The reduced graphene oxide-silver nanoparticles (rGO-AgNPs) were synthesized by the chemical reduction method and characterized by using ultraviolet-visible (UV-vis) absorption, transmission electron microscopy (TEM), X-ray diffractometer (XRD), and scanning probe microscopy (SPM). The binding reaction of rGO-AgNPs with bovine serum albumin (BSA) was investigated by using fluorescence spectrometry and SPM. As the concentration of AgNPs increased, the fluorescence spectrum was quenched, and the quenching process of rGO-AgNPs and BSA was static quenching. Thermodynamic parameters of the absorption process were evaluated at different temperatures, and the negative values of Gibbs free energy (ΔG) showed that this process was spontaneous. The main type of interaction was hydrophobic interaction according to the values of changes in standard enthalpy (ΔH) and entropy (ΔS). In addition, the morphology changes of proteins interacting with nanomaterials were detected by SPM.

1. Introduction

Graphene is a single atomic thick sheet of sp^2 bonded carbon atoms most commonly derived from the exfoliation of graphite [1, 2]. Due to its unique chemical structure and geometry, it has extraordinary physical and chemical properties, including high fracture strength and excellent electrical and thermal conductivity [3, 4]. These properties make it widely used in quantum physics, nanoelectronics, energy research, engineering, and biomaterials [5, 6]. Graphene is composed of a single-layer six-membered ring structure and can be regarded as a planar aromatic polymer. The high surface area of graphene sheets serves as a support for growth and stabilization of nanoparticles which prevents them from aggregating [7–11].

Silver nanoparticles (AgNPs) have broad application prospects in the fields of catalysis, optics, electronics, biomedicine, biosensors, and life medicine due to its special physical and chemical properties [12, 13]. AgNPs have strong bactericidal ability against many types of bacteria such as Neisseria gonorrhoeae, Chlamydia trachomatis, and Escherichia coli, but they do not appear to be resistant. Compared with macroscale silver particles, the sharp increase in the specific surface area of AgNPs increases the chance of contact with bacteria. However, the agglomeration characteristics of nanomaterials affect its stability [14]. Graphene also represents a valuable platform for the development of nanoparticles, which allows the combination of nanomaterials with different properties to give novel materials with improved

or new functionalities. Furthermore, it has a large specific surface area, excellent adsorption capacity, and high chemical stability, which can support AgNPs and increase its stability [15–17]. It has been proved that graphene and AgNPs can produce synergistic reaction and enhance antibacterial effect. Nanoparticles with special properties of graphene and AgNPs are effective medical nanomaterials, which have attracted wide interest [18–23]. Therefore, the formation of nanoparticle-protein corona of graphene oxide-silver nanoparticles with BSA has been investigated in our previous work [24–26].

At present, liquid phase reduction is often used to load silver nanoparticles onto the surface of graphene, but most of them inevitably introduce biotoxic and environmental hazard agents under highly corrosive conditions [27]. In this paper, the reduced graphene oxide-silver nanoparticles (rGO-AgNPs) were prepared and replaced by green nontoxic glucose as a reducing agent to reduce silver anion in graphene oxide [28]. In addition, X-ray diffraction (XRD), UV-vis spectrophotometry, transmission electron microscopy (TEM), and scanning probe microscopy (SPM) were used to characterize rGO-AgNPs. Spectroscopic methods were used to study the interaction between rGO-AgNPs and bovine serum albumin, and the corresponding spectroscopy and thermodynamic data were obtained, which provided a theoretical basis for the wide application of rGO-AgNPs in the medical field.

2. Experimental

2.1. Materials. Graphene oxide (1.0 mg/mL), silver nitrate ($AgNO_3$), and glucose (analytical pure AR) were bought from Sinopharm Chemical Reagent Co., Ltd. Tris (hydroxymethyl)-aminomethane (Tris, ≥99% purity) and ammonia (AR) were both purchased from Alfa Aesar. Bovine serum albumin (BSA, ≥98% purity, Mw = 66.446 kg/mol) was supplied by J&K Scientific Ltd.; the solutions were prepared by the weight method.

2.2. Preparation and Characterization of rGO-AgNPs. Synthesis of graphene-silver nanoparticles (rGO-AgNPs) by the chemical reduction method was as follows: taking 25 mL of graphene oxide with a concentration of 1.0 mg/mL after dialysis, disposing silver ammonia solution, and dissolving 52.5 mg $AgNO_3$ in 2.5 mL deionized water. Then, 3% ammonia was dropped into the silver nitrate aqueous solution until the precipitation just disappeared. The newly configured silver ammonia solution and the graphene oxide aqueous solution were stirred and mixed at 50°C for 30 min, and an aqueous solution containing glucose (0.5 g, 25 mL) was added. The mixed solution was heated to 95°C and stirred for 1 h. After the reaction solution was naturally cooled, the product was separately subjected to centrifugal washing with ethanol and deionized water three times, and the obtained solid was vacuum dried at 60°C for 24 h.

The formation of rGO-AgNPs was confirmed by the plasmon resonance band using ultraviolet-visible spectroscopy (UV-vis, Shimadzu UV-2501PC spectrometer). X-ray diffraction (XRD) was performed using a Shimadzu X-ray diffractometer-6100 with Cu Kα X-ray radiation (40 kV) and scanning in the range of 5° to 80°. The morphology and dispersion of rGO-AgNPs were observed using transmission electron microscopy (TEM) and SPM (Shimadzu SPM-9700). The particle size analysis software (Nano Measurer 1.2) was used to measure the distribution of particle size.

2.3. Fluorescence Analysis on the Interaction. In order to further understand the interaction between rGO-AgNPs and BSA, the fluorescence measurement was carried out using a F-4600 fluorescence spectrophotometer. The parameters of the BSA system were determined as follows: excitation wavelength was set as 280 nm, and scanning range was from 300 nm to 450 nm. The concentration of BSA solution in the cuvette was 2.0 μM. The obtained fluorescence data was processed to draw a Stern-Volmer line, and the thermodynamic parameters of the combined system were determined.

3. Results and Discussion

3.1. Characterization of rGO-AgNPs. RGO-AgNPs have absorption peaks in the ultraviolet-visible region. It is known that the ultraviolet absorption peak of graphene oxide is at around 230 nm and a shoulder peak is at approximately 300 nm due to the electronic π-π^* transitions of C-C aromatic and the n-π^* transitions of C=O bonds, respectively [29] (Figure 1, red line). A new peak at approximately 411 nm is evidently seen after attachment with AgNPs onto the rGO surface (Figure 1, black line), which is the absorption peak of typical spherical silver particles. This result is basically consistent with that reported in the literature [30]. The spectra from the UV-vis spectrophotometry analysis confirmed the presence of AgNP formation for the nanoparticles. Therefore, it can be preliminarily concluded that the nanoparticles were synthesized.

In the XRD pattern of Figure 2, the diffraction peaks appear at 38.08°, 44.16°, 64.44°, and 77.44°, corresponding to the (111), (200), (220), and (311) diffraction peaks of fcc Ag [26]. The results were basically consistent with the literature, indicating that the graphene oxide added with $AgNO_3$ is reduced by glucose to form graphene-silver nanoparticles. The morphology of rGO-AgNPs was investigated by TEM. It can be seen from Figure 3 that the nanosilver is spherical and the scale distribution is uniform. The average particle size can be obtained by the particle size analysis software, which is 6.41 nm. This result is in accordance with the average particle size of 6.52 nm obtained by SPM scanning analysis in Figure 4.

3.2. SPM Analysis of the Interaction of rGO-AgNPs with BSA. To further investigate the interaction of BSA and rGO-AgNPs, the surface morphology of the system was analyzed by SPM, which is a very reliable tool for biological applications [26, 31, 32]. The SPM image clearly showed that BSA molecules adsorbed onto mica (Figure 5(a)). It can be seen that the molecules of BSA appear to be more compact and to aggregate around rGO-AgNPs' surface after the binding

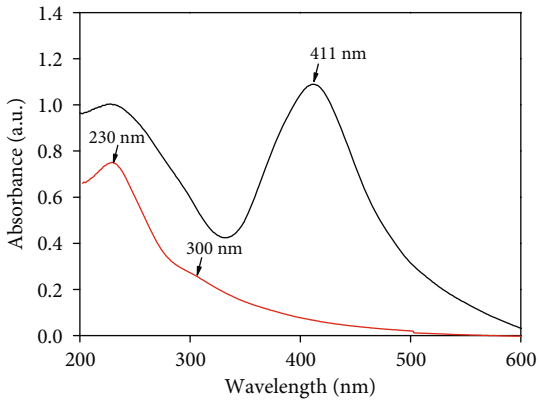

Figure 1: UV-vis spectra of GO (red line) and rGO-AgNPs (black line).

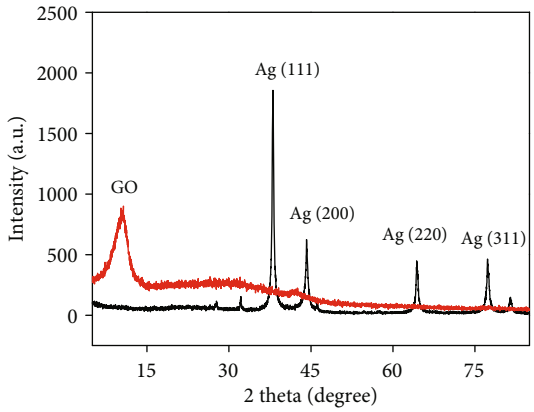

Figure 2: X-ray diffraction pattern of GO and rGO-AgNPs.

process (Figure 5(b)). In addition, the nanomaterial can change the structure of BSA.

3.3. Temperature-Dependent Fluorescence Analysis. The quenching mechanism between quenchers and proteins can be divided into dynamic quenching and static quenching [33]. Static quenching is a process in which a quencher molecule and a fluorescent substance molecule form a nonfluorescent complex in a ground state; thereby, the fluorescence intensity of the fluorescent substance is reduced. Dynamic quenching is the fluorescence quenching caused by the collision between the quencher molecule and the excited state molecules of the fluorescent molecule. If the biomolecular quenching constant (K_q) is more than the value of the maximum collisional quenching constant ($2.0 \times 10^{10}\,\mathrm{L \cdot mol^{-1} \cdot s^{-1}}$), static quenching is dominant, whereas dynamic quenching is not dominant. The quenching mode can be expressed by the Stern-Volmer equation:

$$\frac{F_0}{F} = 1 + K_{sv}[Q] = 1 + K_q \tau_0 [Q], \tag{1}$$

where K_q represents the biomolecular quenching constant of the quenching process, K_{sv} represents the Stern-Volmer quenching constant, and τ_0 is the average lifetime of the

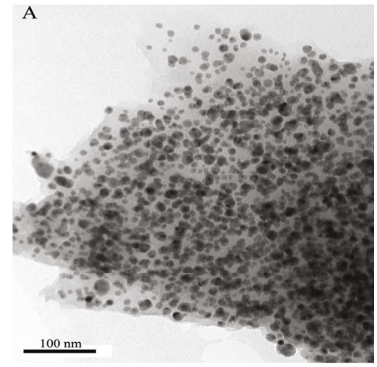

(a)

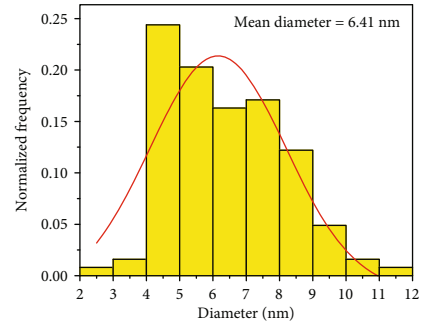

(b)

Figure 3: (a) Transmission electron micrograph of rGO-AgNPs; (b) size distribution of silver nanoparticles attached to rGO sheets.

fluorescent molecule in the absence of the quencher. The fluorescence lifetime of BSA is about 10^{-8} s. F_0 and F are the fluorescence intensities of BSA in the absence and presence of rGO-AgNPs, respectively. $[Q]$ is the concentration of the quencher [26]. Based on fluorescence data obtained at two different temperatures (303 K and 308 K, see Figure 6), the Stern-Volmer plots are shown in Figure 7, and the corresponding values are listed in Table 1. It can be seen from Figures 6(a) and 6(b) that the BSA fluorescence intensity is lowered by increasing the temperature. The values of K_q were greater than $2.0 \times 10^{10}\,\mathrm{L \cdot mol^{-1} \cdot s^{-1}}$, indicating that the combination of rGO-AgNPs and BSA is a static quenching process.

The relationship between the concentration of rGO-AgNPs and the fluorescence intensity can be quantified by the Hill equation (Equation (2)) [34]:

$$\log\left[\frac{(F_0 - F)}{F}\right] = \log K_a + n \log [Q]. \tag{2}$$

The Hill coefficient (n) represents the degree of cooperativity for the protein binding onto the material surface. In most cases, n is greater than 1, suggesting cooperative binding of BSA to the surface of GO-AgNCPs [26]. The binding of a ligand is weakened when n is less than 1; in contrast, that

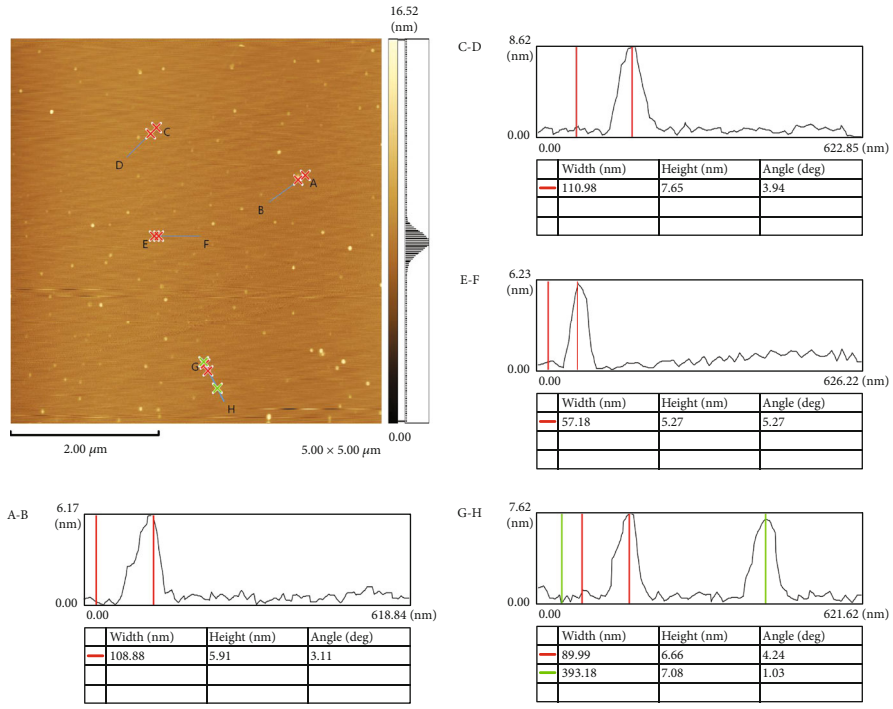

Figure 4: Dynamic mode SPM images of rGO-AgNPs.

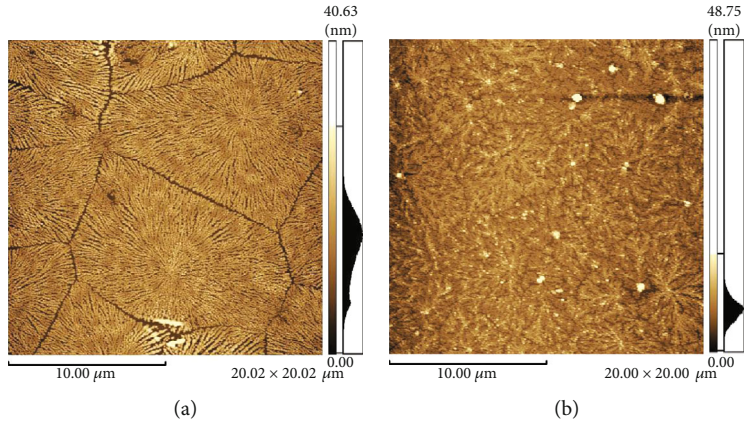

Figure 5: SPM images of BSA (a) and the BSA-rGO-AgNP system (b) on mica.

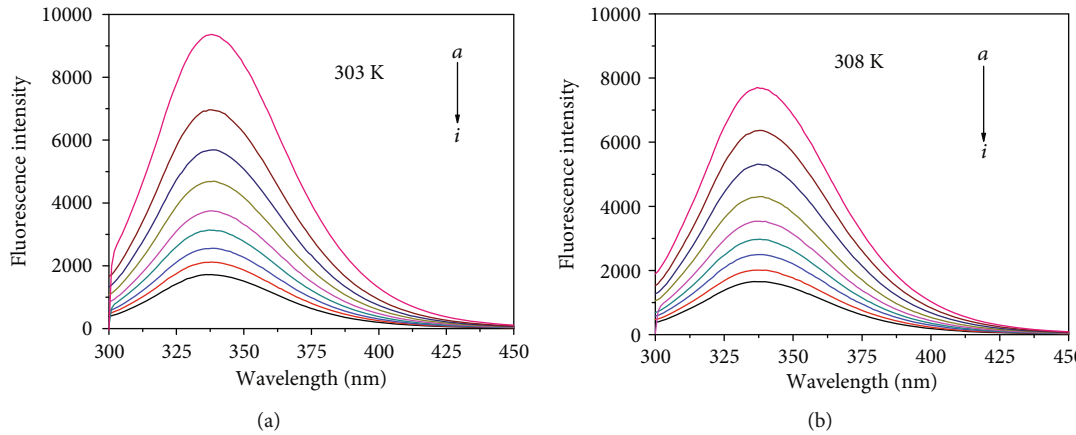

Figure 6: Fluorescence quenching of BSA under varying concentrations of rGO-AgNPs at (a) 303 K and (b) 308 K.

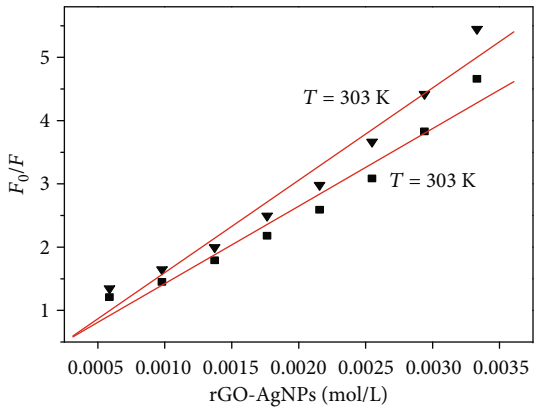

Figure 7: The plot of F_0/F versus [Q] of the BSA-rGO-AgNP system.

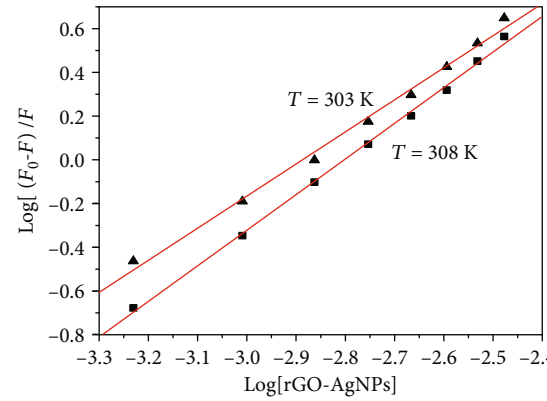

Figure 8: Hill plots for the BSA-rGO-AgNP system.

Table 1: The quenching constants.

T (K)	K_{sv} ($\times 10^3$ L·mol^{-1})	K_q ($\times 10^{11}$ L·mol^{-1}·s^{-1})	R
303	1.46 ± 0.04	2.53 ± 0.04	0.9578
308	1.23 ± 0.02	2.12 ± 0.04	0.9537

Table 2: Binding parameters of the BSA-rGO-AgNP system.

T (K)	K_a ($\times 10^3$ L·mol^{-1})	n	R
303	4.24 ± 0.08	1.47 ± 0.06	0.9921
308	4.57 ± 0.07	1.63 ± 0.05	0.9970

Table 3: Thermodynamic parameters of the BSA-rGO-AgNP system.

T (K)	ΔH (kJ·mol^{-1})	ΔG (kJ·mol^{-1})	ΔS (J·mol^{-1}·K^{-1})
303	116.83	-24.59 ± 0.12	466.74
308		-26.93 ± 0.16	

is strengthened if there are already other ligands adsorbed to the surface. In addition, it is independent of other ligands already at the surface when $n = 1$ [35]. The values of K_a and n can be obtained from the intercept and slope of the fitting straight line (see Figure 8) and are listed in Table 2. The binding constant (K_a) values calculated for 303 K and 308 K are $(4.24 \pm 0.08) \times 10^3$ L · mol^{-1} and $(4.57 \pm 0.07) \times 10^3$ L·mol^{-1}, respectively. K_a becomes greater with rising temperature, indicating that the binding process is endothermic. In this experiment, $n > 1$ at two temperatures means that once a protein molecule is adsorbed onto the nanoparticle surface, the binding of other protein molecules to the surface is enhanced in a super-linear way.

The values of enthalpy (ΔH) can be considered as a constant when there is no great change in temperature. The thermodynamic parameters can be obtained using the following formulas:

$$\ln\left(\frac{K^2}{K^1}\right) = \frac{\Delta H}{R}\left(\frac{1}{T^1} - \frac{1}{T^2}\right), \quad (3)$$

$$\Delta G = \Delta H - T\Delta S = -RT \ln K, \quad (4)$$

where ΔH, ΔG, and ΔS are enthalpy change, Gibbs free energy change, and entropy change, respectively; K represents the associative binding constants at the corresponding temperature; and R is the gas constant (8.314 J/mol/K). Results were gathered in Table 3. ΔG involved in the complex formation process was evaluated as -24.59 ± 0.12 kJ · mol^{-1} and -26.93 ± 0.16 kJ · mol^{-1} for the two temperatures. The values of ΔG are less than zero which indicates that the reaction is spontaneous. $\Delta H > 0$ and $\Delta S > 0$ reveal that this adsorption process is endothermic and mainly driven by entropy. The hydrophobic interaction plays an important role in the processes according to the results.

4. Conclusions

In this paper, rGO-AgNPs were prepared by the chemical reduction method and characterized by spectroscopy. The UV-vis spectra and XRD pattern were measured to indicate the formation of rGO-AgNPs. The TEM, SEM, and SPM scans indicated that the nanosilver particles were supported on the graphene sheets and the particle size was uniform. Based on the synthesis of the desired graphene-silver nanoparticles, various methods were used to systematically study the interaction of graphene-silver nanoparticles with BSA in buffer solution (pH = 7.21). After rGO-AgNPs react with BSA, nanoparticles rapidly adsorb proteins on their surface and the particle size of the nanosilver increases. The binding process of BSA onto the surface of rGO-AgNPs is static quenching. Judging from entropy change, the main force between rGO-AgNPs and BSA is hydrophobic interaction and the reaction proceeds is spontaneous.

Data Availability

The data used to support the findings of this study are included within the article.

Conflicts of Interest

The authors declare that they have no conflicts of interest.

Authors' Contributions

Huali Zhang and Wen Liu are coauthors.

Acknowledgments

The authors are grateful to the National Natural Science Foundation of China (Nos. 81502255 and 21603084), the Natural Science Foundation of Shandong Province (Nos. ZR2017BB015, ZR2016BP10, and ZR2018PB011), the Medicine and Health Project of Shandong Province (No. 2016WS0164), the Higher Education Research Project of Shandong Province (No. J17KB065), School Support Foundation of Jining Medical University (No. JY2017KJ042), NSFC cultivation project of Jining Medical University (Nos. JYP2018KJ03 and JYP2018KJ17), Staring Foundation of Affiliated Hospital of Jining Medical University (No. 2016-BS-009), Science and Technology Development Plan Foundation of Jining (No. 2014jnjc09), School-Level University Student Research Project (No. JYXS2017KJ007), National College/School-Level Students Innovation and Entrepreneurship Training Program (Nos. cx2018008 and 201810443008).

References

[1] A. Gholampour, M. V. Kiamahalleh, D. N. H. Tran, T. Ozbakkaloglu, and D. Losic, "From graphene oxide to reduced graphene oxide: impact on the physiochemical and mechanical properties of graphene-cement composites," *ACS Applied Materials & Interfaces*, vol. 9, no. 49, pp. 43275–43286, 2017.

[2] M. Miscuglio, D. Spirito, R. P. Zaccaria, and R. Krahne, "Shape approaches for enhancing plasmon propagation in graphene," *ACS Photonics*, vol. 3, no. 11, pp. 2170–2175, 2016.

[3] S. Fazil, M. Bangesh, W. Rehman et al., "Mechanical, thermal, and dielectric properties of functionalized graphene oxide/polyimide nanocomposite films," *Nanomaterials and Nanotechnology*, vol. 9, 2019.

[4] A. Ejigu, I. A. Kinloch, and R. A. W. Dryfe, "Single stage simultaneous electrochemical exfoliation and functionalization of graphene," *ACS Applied Materials & Interfaces*, vol. 9, no. 1, pp. 710–721, 2017.

[5] Z. Wang, T. Li, L. Schulte, K. Almdal, and S. Ndoni, "Photocatalytic nanostructuring of graphene guided by block copolymer self-assembly," *ACS Applied Materials & Interfaces*, vol. 8, no. 13, pp. 8329–8334, 2016.

[6] K. E. Whitener Jr., R. Stine, J. T. Robinson, and P. E. Sheehan, "Graphene as electrophile: reactions of graphene fluoride," *Journal of Physical Chemistry C*, vol. 119, no. 19, pp. 10507–10512, 2015.

[7] M. Yu, P.-R. Liu, Y.-J. Sun, J.-H. Liu, J.-W. An, and S.-M. Li, "Fabrication and characterization of Graphene-Ag Nanoparticles composites," *Journal of Inorganic Materials*, vol. 27, no. 1, pp. 89–94, 2012.

[8] D. Chen, H. B. Feng, and J. H. Li, "Graphene oxide: preparation, functionalization, and electrochemical applications," *Chemical Reviews*, vol. 112, no. 11, pp. 6027–6053, 2012.

[9] P. Liu, J. Ma, S. Deng et al., "Graphene-Ag nanohexagonal platelets based ink with high electrical properties at low sintering temperatures," *Nanotechnology*, vol. 27, no. 38, pp. 385603–385612, 2016.

[10] Y. Wang, Z. Li, J. Wang, J. Li, and Y. Lin, "Graphene and graphene oxide: biofunctionalization and applications in biotechnology," *Trends in Biotechnology*, vol. 29, no. 5, pp. 205–212, 2011.

[11] J. Lu, P. S. E. Yeo, Y. Zheng et al., "Using the graphene Moiré pattern for the trapping of C_{60} and homoepitaxy of graphene," *ACS Nano*, vol. 6, no. 1, pp. 944–950, 2012.

[12] J. Li, M. Wang, G. Liu et al., "Enhanced iodide removal from water by nano-silver modified anion exchanger," *Industrial and Engineering Chemistry Research*, vol. 57, no. 51, pp. 17401–17408, 2018.

[13] M. Khatami, H. Q. Alijani, and I. Sharifi, "Biosynthesis of bimetallic and core-shell nanoparticles: their biomedical applications - a review," *IET Nanobiotechnology*, vol. 12, no. 7, pp. 879–887, 2018.

[14] Y. K. Liu and M. T. Lee, "Laser direct synthesis and patterning of silver nano/microstructures on a polymer substrate," *ACS Applied Materials & Interfaces*, vol. 6, no. 16, pp. 14576–14582, 2014.

[15] M. S. Nejad, G. H. S. Bonjar, M. Khatami, A. Amini, and S. Aghighi, "In vitro and in vivo antifungal properties of silver nanoparticles against Rhizoctonia solani, a common agent of rice sheath blight disease," *IET Nanobiotechnology*, vol. 11, no. 3, pp. 236–240, 2017.

[16] A. Ivask, N. H. Voelcker, S. A. Seabrook et al., "DNA melting and genotoxicity induced by silver nanoparticles and graphene," *Chemical Research in Toxicology*, vol. 28, no. 5, pp. 1023–1035, 2015.

[17] J. Wang, X. Zhao, J. Li et al., "Electrostatic assembly of peptide nanofiber-biomimetic silver nanowires onto graphene for electrochemical sensors," *ACS Macro Letters*, vol. 3, no. 6, pp. 529–533, 2014.

[18] X. Meng, H. Wang, N. Chen et al., "A graphene-silver nanoparticle-silicon sandwich SERS chip for quantitative detection of molecules and capture, discrimination, and inactivation of bacteria," *Analytical Chemistry*, vol. 90, no. 9, pp. 5646–5653, 2018.

[19] T. Mahmoudi, Y. Wang, and Y. B. Hahn, "Stability enhancement in perovskite solar cells with perovskite/silver-graphene composites in the active layer," *ACS Energy Letters*, vol. 4, no. 1, pp. 235–241, 2019.

[20] J. Jung, G. M. Raghavendra, D. Kim, and J. Seo, "One-step synthesis of starch-silver nanoparticle solution and its application to antibacterial paper coating," *International Journal of Biological Macromolecules*, vol. 107, no. 23, pp. 2285–2290, 2018.

[21] S. Kellici, J. Acord, A. Vaughn et al., "Calixarene assisted rapid synthesis of silver-graphene nanocomposites with enhanced antibacterial activity," *ACS Applied Materials & Interfaces*, vol. 8, no. 29, pp. 19038–19046, 2016.

[22] K.-H. Tseng, C.-J. Chou, S.-H. Shih, D.-C. Tien, H.-C. Ku, and L. Stobinski, "Comparison of graphene impregnated with/without nanosilver prepared by submerged arc discharge method," *Nanomaterials and Nanotechnology*, vol. 8, 2018.

[23] L. A. V. de Luna, A. C. M. de Moraes, S. R. Consonni et al., "Comparative in vitro toxicity of a graphene oxide-silver nanocomposite and the pristine counterparts toward macrophages," *Journal of Nanobiotechnology*, vol. 14, no. 1, 2016.

[24] X. Xu, Z. Du, W. Wu et al., "Synthesis of triangular silver nanoprisms and spectroscopic analysis on the interaction with bovine serum albumin," *Analytical and Bioanalytical Chemistry*, vol. 409, no. 22, pp. 5327–5336, 2017.

[25] X. Y. Xu, Y. F. Wang, H. Wang et al., "Synthesis of triangular silver nanoprisms and studies on the interactions with human serum albumin," *Journal of Molecular Liquids*, vol. 220, pp. 14–20, 2016.

[26] X. Y. Xu, X. Y. Mao, Y. F. Wang et al., "Study on the interaction of graphene oxide-silver nanocomposites with bovine serum albumin and the formation of nanoparticle-protein corona," *International Journal of Biological Macromolecules*, vol. 116, pp. 492–501, 2018.

[27] W. Lai, W. Zhao, and X. Li, "Research progress on controllable synthesis of multi-morphology nanosilver," *Rare Metal Materials and Engineering*, vol. 7, no. 40, pp. 1311–1316, 2011.

[28] W. Shao, X. Liu, H. Min, G. Dong, Q. Feng, and S. Zuo, "Preparation, characterization, and antibacterial activity of silver nanoparticle-decorated graphene oxide nanocomposite," *ACS Applied Materials & Interfaces*, vol. 7, no. 12, pp. 6966–6973, 2015.

[29] A. F. de Faria, F. Perreault, E. Shaulsky, L. H. Arias Chavez, and M. Elimelech, "Antimicrobial electrospun biopolymer nanofiber mats functionalized with graphene oxide-silver nanocomposites," *ACS Applied Materials & Interfaces*, vol. 7, no. 23, pp. 12751–12759, 2015.

[30] Z. Zhang, F. Xu, W. Yang et al., "A facile one-pot method to high-quality Ag-graphene composite nanosheets for efficient surface-enhanced Raman scattering," *Chemical Communications*, vol. 47, no. 22, pp. 6440–6442, 2011.

[31] Y. Yang, H. Wang, and D. A. Erie, "Quantitative characterization of biomolecular assemblies and interactions using atomic force microscopy," *Methods*, vol. 29, no. 2, pp. 175–187, 2003.

[32] G. Zhang, L. Wang, and J. Pan, "Probing the binding of the flavonoid diosmetin to human serum albumin by multispectroscopic techniques," *Journal of Agricultural and Food Chemistry*, vol. 60, no. 10, pp. 2721–2729, 2012.

[33] Y. J. Hu, Y. Ou-Yang, C. M. Dai, Y. Liu, and X. H. Xiao, "Site-selective binding of human serum albumin by palmatine: spectroscopic approach," *Biomacromolecules*, vol. 11, no. 1, pp. 106–112, 2010.

[34] D. Sarkar, "Probing the interaction of a globular protein with a small fluorescent probe in the presence of silver nanoparticles: spectroscopic characterization of its domain specific association and dissociation," *RSC Advances*, vol. 3, no. 46, pp. 24389–24399, 2013.

[35] S. P. Boulos, T. A. Davis, J. A. Yang et al., "Nanoparticle-protein interactions: a thermodynamic and kinetic study of the adsorption of bovine serum albumin to gold nanoparticle surfaces," *Langmuir*, vol. 29, no. 48, pp. 14984–14996, 2013.